Supplemental

22rv1 and 22rv1×PSCA models

22rv1 and 22rv1×PSCA cell lines were transfected with Firefly Luciferase (Fluc)-IRES-mCherry and FLuc-IRES-GFP respectively using lentiviral transfection in conjunction with UCLA's Vector Core (1). The 22rv1 derived cell lines were cultured in RPMI 1640 supplemented with 10% FBS and 1% Penicillin and Streptomycin. The transfected cells were stained with 1G8 murine anti-PSCA antibody, followed by Dylight 647 conjugated Goat anti-mouse Fc_γ-specific secondary antibody (Jackson ImmunoResearch) and were sorted twice by FACS to create 22rv1 FLuc-IRES-mCherry and 22rv1×PSCA FLuc-IRES-GFP cell lines that stably expressed their fluorescent markers through more than 12 passages. The 22rv1×PSCA FLuc-IRES-GFP line was simultaneously sorted for the highly PSCA expressing cell population.

Lentiviral transfection of 22rv1 with FLuc-IRES-mCherry and 22rv1×PSCA with Fluc-IRES-GFP created PSCA positive and negative cell lines with stable expression of FLuc (Supplemental Figure 1 A). Quantitative flow cytometry ($n = 3$) shows expression of $2.3\times10^6 \pm 5.1\times10^5$ mean PSCA antigens per cell on 22rv1×PSCA FLuc-IRES-GFP cells and 3900 ± 3600 mean PSCA antigens per cell on 22rv1 FLuc-IRES-mCherry cells.

Tumor growth was followed in mice bearing firefly luciferase transfected 22rv1 and 22rv1×PSCA tumors beginning 5-7 days post-injection by optical imaging. 150mg/kg of D-Luciferin (GoldBio) in 100μL of PBS was injected intraperitoneally and following a 15 minute uptake period the mice were imaged in an IVIS Lumina II cooled CCD optical imager (Caliper Life Sciences). Only mice showing a signal on optical imaging received bone scans and immunoPET imaging.

Take rates for 22rv1 intratibial xenografts were high (5/7) but 22rv1×PSCA were exceedingly low (2/36) despite extensive troubleshooting including varying the mouse strain (Nude $n = 32$, SCID $n = 4$), the cell line (22rv1×PSCA $n = 4$, 22rv1×PSCA FLuc-IRES-GFP $n = 32$), and the number of cells injected (1×10^5–3×10^5). Only one mouse with a 22rv1×PSCA intratibial tumor was able to be imaged. A subset of the remaining mice had a tumor grow in the muscle surrounding the tibia due to a missed injection (5/36), but the majority of the mice showed no signal on optical imaging and never developed a tumor (25/36). The reason for the low intratibial tumor take rate in PSCA transfected 22rv1 cell lines is unknown especially considering that 22rv1 FLuc-IRES-mCherry not transfected with PSCA had a much higher rate of intratibial establishment (5 out of 7 mice, with 1 mouse growing a muscle tumor, and 1 mouse showing no signal on optical imaging) and that both 22rv1 and 22rv1×PSCA have 100% take rates for subcutaneous xenografts.

Histology of 22rv1 and 22rv1×PSCA mice confirmed a mixed osteolytic and osteoblastic tumor phenotype in-line with previous reports (Supplemental Figure 2) (2, 3). Bone scans of the 22rv1 and 22rv1×PSCA mice, show consistent increases in the intratibial xenograft bearing tibia at 6 weeks post-xenograft-injection (Supplemental Figures 3 and 4). However, the high uptake in the knee and rest of the skeleton illustrates the lack of specificity of this imaging modality and the difficulty of distinguishing true and false positives.

The one mouse with a histologically confirmed intratibial 22rv1×PSCA tumor showed higher uptake in the 22rv1×PSCA bearing tibia compared to the sham tibia control at two weeks and six weeks post-injection by immunoPET (Supplemental Figure 4). Biodistribution of this mouse at 6 weeks post-injection showed uptake of 3.31%ID/g for the 22rv1×PSCA tibia, 46.9 times higher than the sham tibia, 8.5 times higher than tibias bearing 22rv1 tumors, and 10.7 times higher than blood despite the excess weight of bone and other non-tumor tissue in the tibia (Supplemental Table 1). Significance testing of the 22rv1×PSCA tibial uptake ($n = 1$) against the distributions for the 22rv1 tibias ($n = 5$) and the pooled sham tibias ($n = 6$) by one-way ANOVA shows significantly increased uptake ($p < 0.0001$) uptake in the 22rv1×PSCA tibia in both cases despite the small sample size.

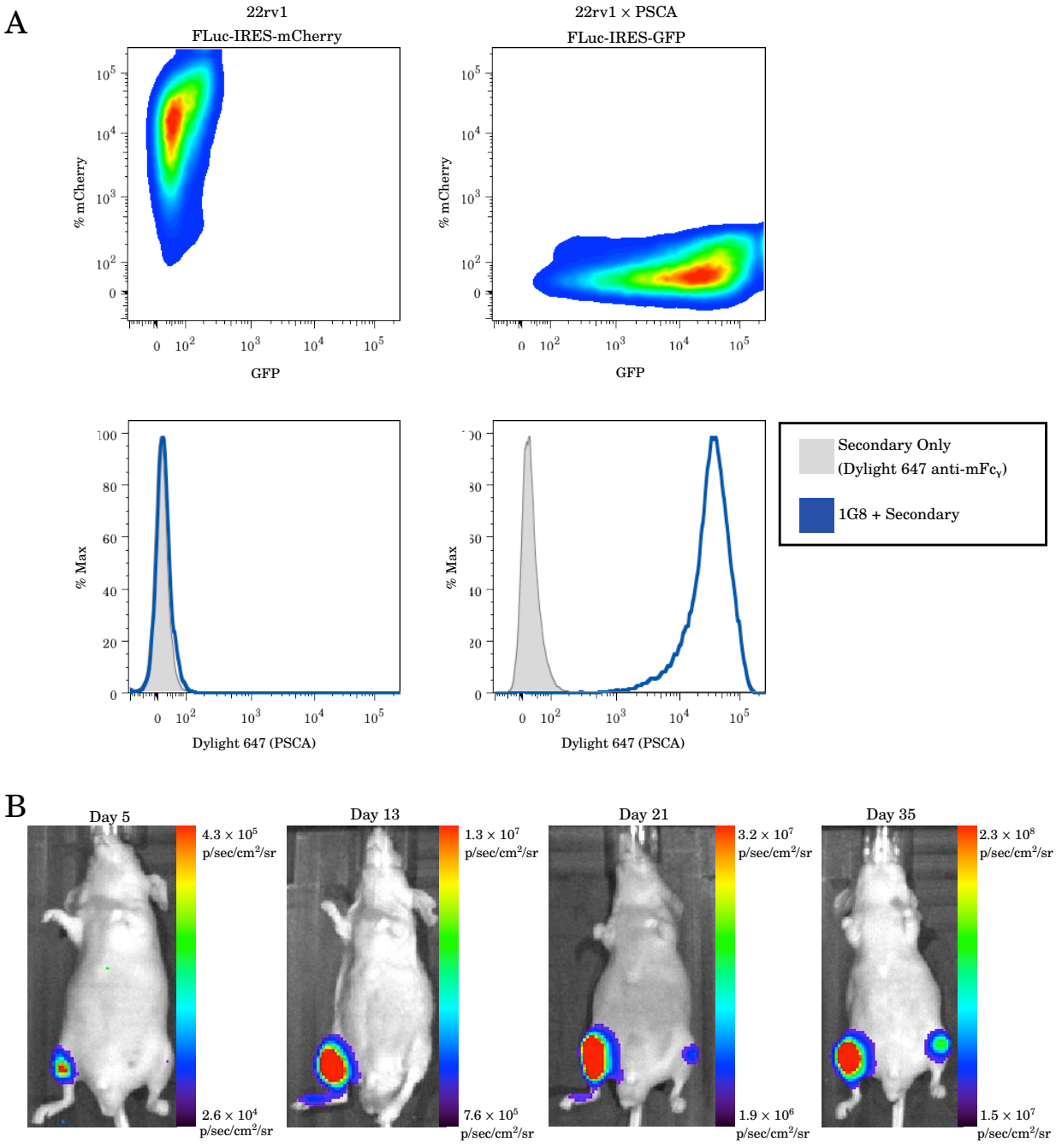

Supplemental Figure 1: Transfection of 22rv1 with FLuc-IRES-mCherry and 22rv1×PSCA with Fluc-IRES-GFP and FACS sorting created FLuc expressing PSCA positive and negative cell lines (A). Expression of Fluc allows for monitoring of tumor growth by optical imaging with both 22rv1 FLuc-IRES-mCherry (left leg) and 22rv1×PSCA FLuc-IRES-GFP (right leg) intratibial xenografts (B).

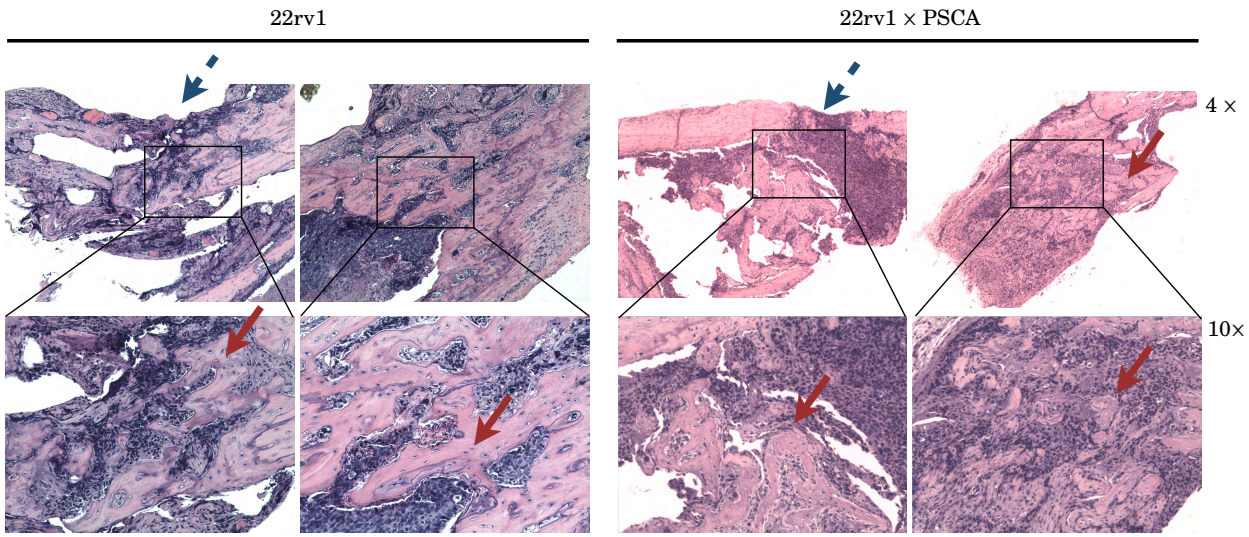

Supplemental Figure 2: H&E Staining of 22rv1 and 22rv1×PSCA intratibial xenografts shows mixed osteolytic (blue dashed arrows) and osteoblastic (solid red arrows) type tumor formation.

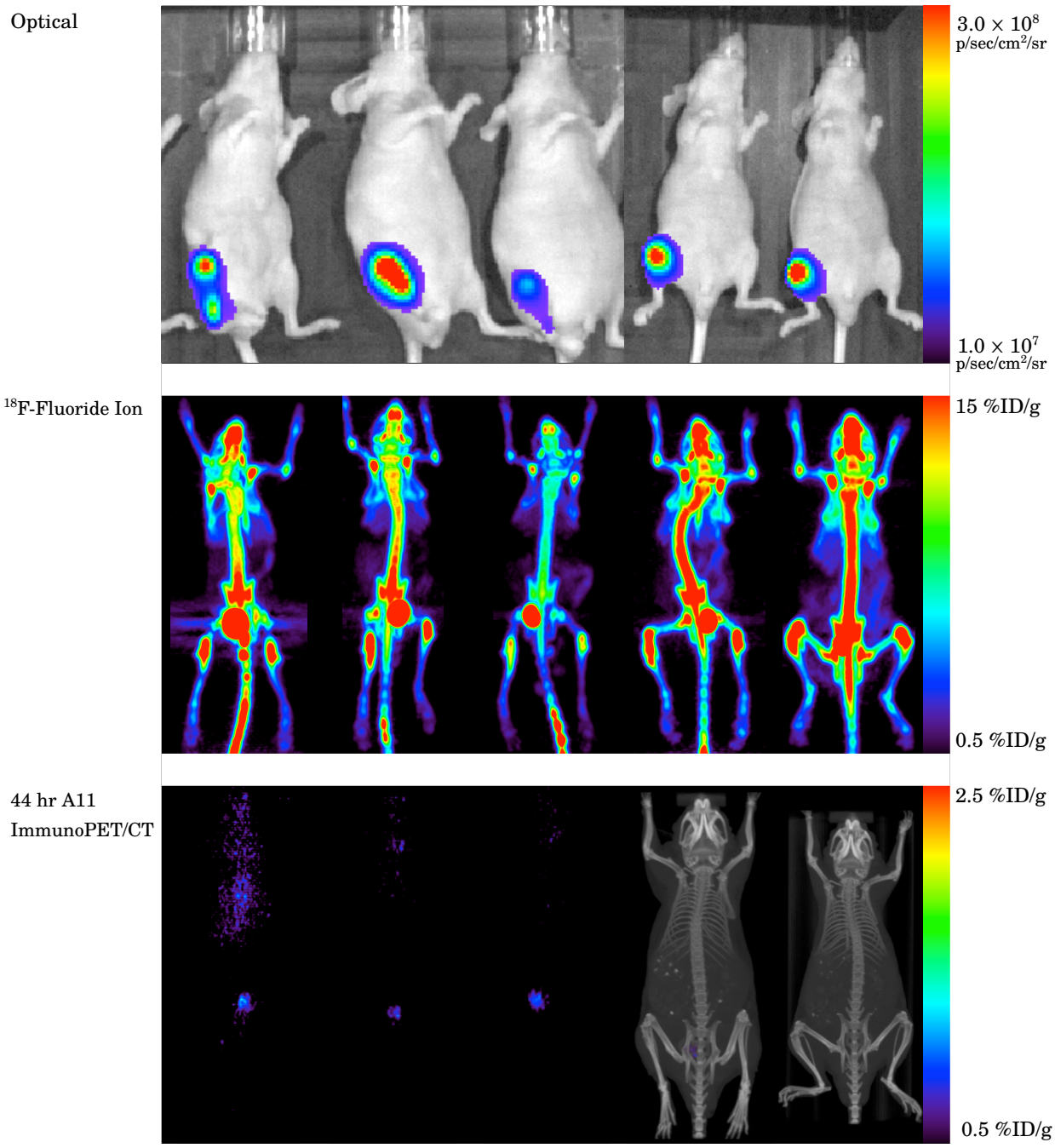

Supplemental Figure 3: Comparison of optical imaging, ^{18}F-Fluoride Bone Scan, and A11 immunoPET in mice bearing 22rv1 intratibial xenograft 6 weeks post-xenograft-implantation. ^{18}F-Fluoride bone scans show increased uptake in the tumor bearing tibia, but with significant background. A11 minibody immunoPET, however, shows no uptake in the 22rv1 intratibial tumor indicating the uptake in 22rv1×PSCA and LAPC-9 mice is antigen specific. Three of the A11 immunoPET scans are shown as full thickness maximum intensity projections of the microPET data only due to a CT scanner malfunction.

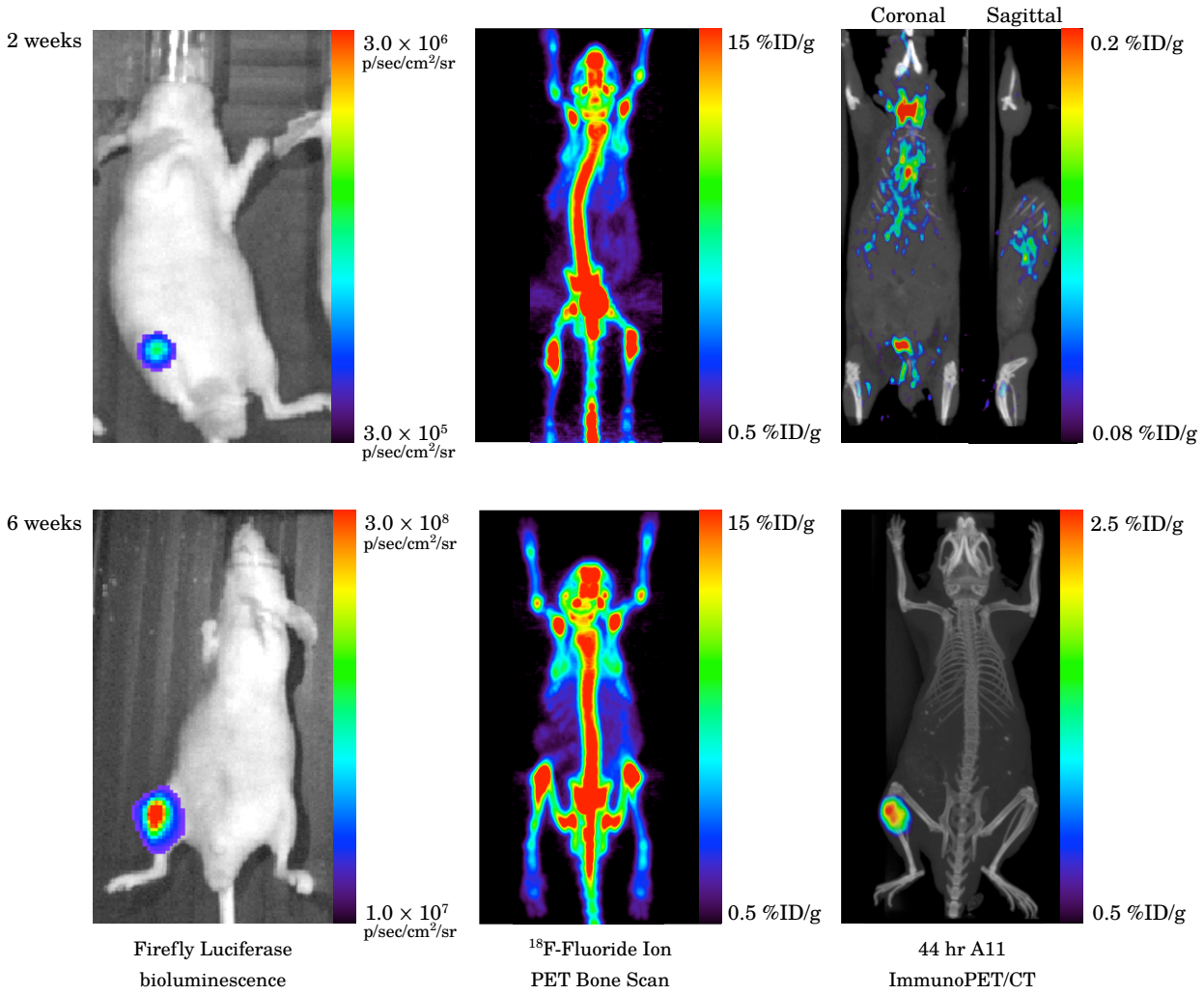

Supplemental Figure 4: Comparison of optical imaging, ^{18}F-Fluoride Bone Scan, and A11 immunoPET in a mouse bearing a 22rv1×PSCA intratibial xenograft at 2 and 6 weeks post-xenograft-implantation. At 2 weeks post-injection, no appreciable increase in uptake can be observed in the tibia bearing the 22rv1×PSCA xenograft with the ^{18}F-Fluoride bone scan while a small increase in intramedullary uptake in the tumor bearing tibia can be seen by 44 hr A11 immunoPET. At 6 weeks post-xenograft implantation, both ^{18}F-Fluoride bone scans and A11 immunoPET show increased uptake in the tumor bearing tibia. However, the signal is much easier to distinguish in the A11 immunoPET scan due to the higher specificity of the radiotracer and lower background in normal tissue. The 2 week A11 immunoPET image is displayed as a 2 mm thick coronal slice through both tibias with a corresponding 2 mm thick sagittal slice through the left tibia as the intramedullary signal is too low to be displayed on a full thickness maximum intensity projection.

	22rv1 ($n = 5$) Intratibial Tumor %ID/g $\pm$ SD	22rv1$\times$PSCA ($n = 1$) Intratibial Tumor %ID/g
Blood	0.40 ± 0.11	0.31
Positive (Left) Tibia	0.36 ± 0.19	3.31
Left Calf Muscle	0.11 ± 0.06	0.93
Left Femur	0.07 ± 0.02	0.10
Negative (Right) Tibia	0.08 ± 0.02	0.07
Right Calf Muscle	0.05 ± 0.02	0.05
Right Femur	0.07 ± 0.02	0.05
Liver	0.14 ± 0.01	0.11
Kidney	0.24 ± 0.05	0.19
Carcass	0.09 ± 0.03	0.08
Pos Tibia:Blood		10.71
Pos Tibia:Neg Tumor Tibia		9.20
Pos Tibia: Sham Tibia		46.86
Pos Tibia:Negative Muscle		70.04

Supplemental Table 1: 44 hour biodistribution of mice bearing 22rv1 and 22rv1$\times$PSCA intratibial xenografts

Histologic analysis of control and MDV-3100 treated tumors

After the last imaging time point and weighing of tumors for biodistribution, tumor samples were fixed in 10% phosphate buffered formalin before gamma-counting. These tumors were then stored in formalin for ≥ 42 days until ^{124}I activity was undetectable. They were then paraffin embedded, sectioned, H&E stained, and slide scanned. The percent of tumor necrosis in each histologic section was calculated using Fiji ("Fiji is Just ImageJ") using a macro partially generated via the Threshold Colour ImageJ plugin to select necrotic tumor regions with a large predominance of eosin staining (5 (4–6). The percent necrosis was calculated by the number of thresholded pixels in the necrotic image divided by the number of thresholded pixels in the total tumor image.

Quantification of necrotic area in H&E staining of LAPC-9 tumors treated with either vehicle control or MDV-3100 (6 A) shows no difference in necrosis between the two groups (15.8 $\pm$ 7.4% Vehicle, 11.2% $\pm$6.2% MDV-3100, $p = 0.20$, 6 B). Regression analysis of the % Necrotic tissue versus A11 minibody uptake shows positive but non-significant correlation for both Vehicle ($r^2 = 0.38, p = 0.10$) and MDV-3100 treated tumors ($r^2 = 0.12, p = 0.39$).

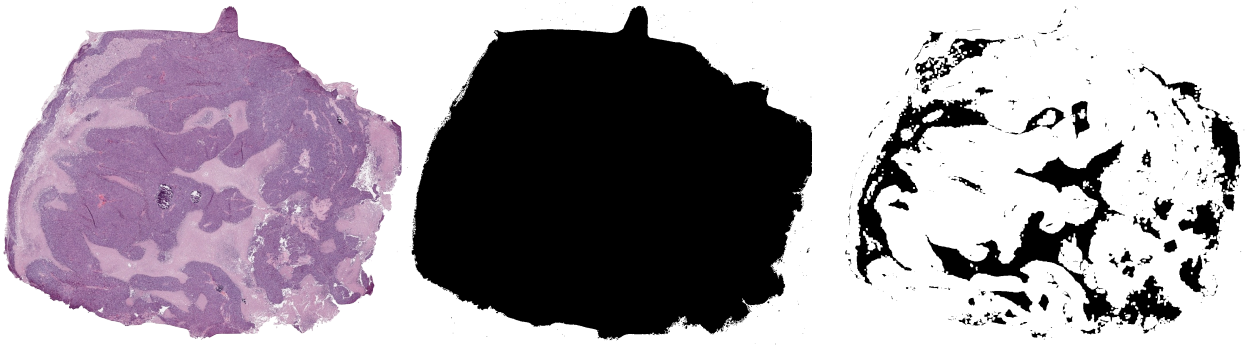

Supplemental Figure 5: Quantification of tumor necrosis using ImageJ based color segmentation. Percent necrosis was calculated as the number of black pixels in the Necrotic image divided by the number of black pixels in the Total Tumor image.

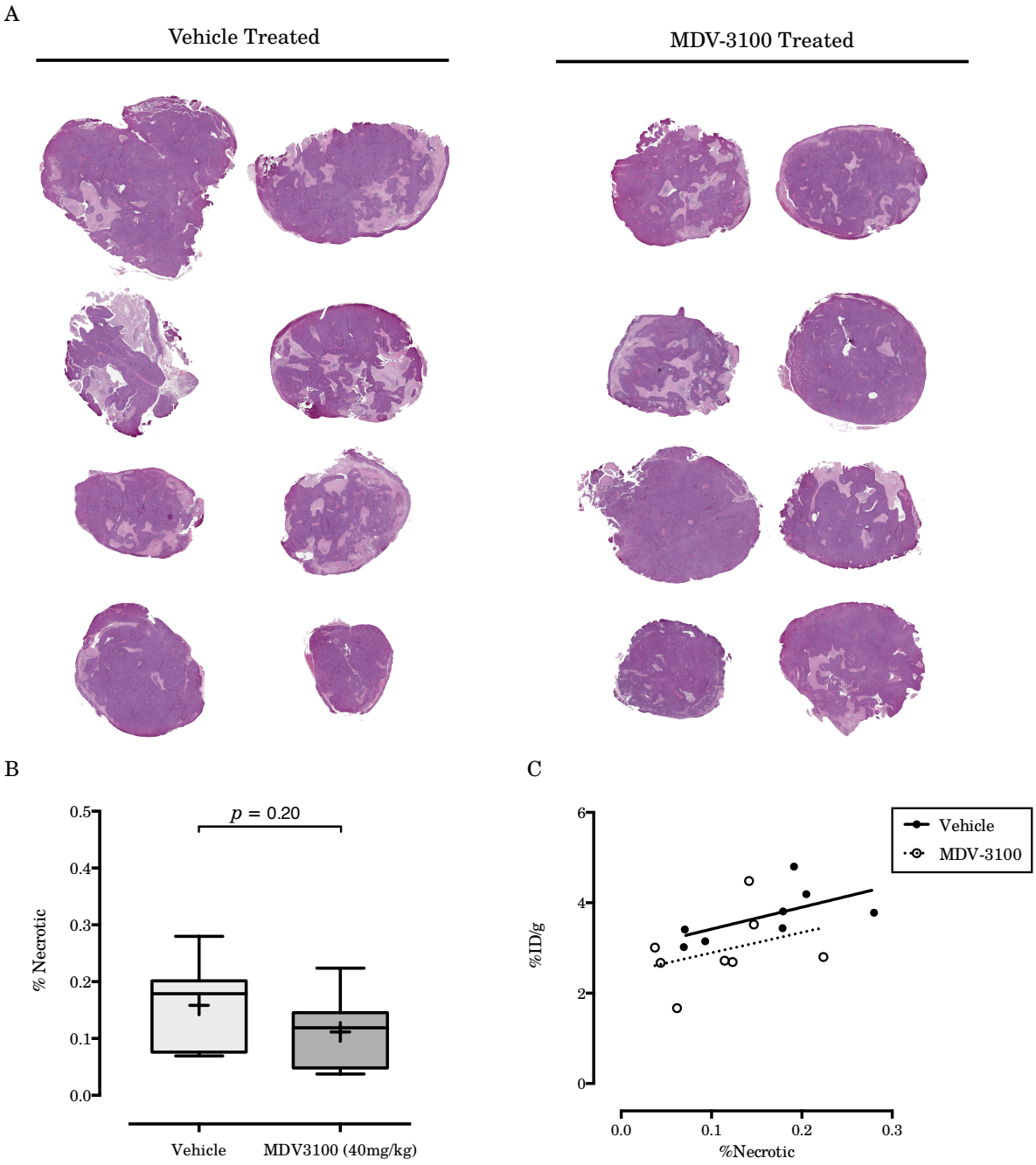

Supplemental Figure 6: H&E staining of LAPC-9 tumors treated with either MDV-3100 or vehicle control (A). Quantification of the % Necrotic tissue in each tumor (B). Regression analysis of the relationship between % Necrotic tissue and tumor uptake of A11 minibody (C).

Bibliography

[1] Knowles SM, Zettlitz KA, Tavare R, Rochefort MM, Salazar FB, Stout DB, *et al*. Quantitative ImmunoPET of Prostate Cancer Xenografts with 89Zr- and 124I-Labeled Anti-PSCA A11 Minibody. J Nucl Med. 2014;55:452–459.

[2] Drake JM, Gabriel CL, Henry MD. Assessing tumor growth and distribution in a model of prostate cancer metastasis using bioluminescence imaging. Clinical & experimental metastasis. 2005;22:674–684.

[3] Henry MD, Silva MD, Wen S, Siebert E, Solin E, Chandra S, *et al*. Spiculated periosteal response induced by intraosseous injection of 22Rv1 prostate cancer cells resembles subset of bone metastases in prostate cancer patients. Prostate. 2005;65:347–354.

[4] Landini G. *Threshold Colour ImageJ Plugin*.

[5] Schneider CA, Rasband WS, Eliceiri KW. NIH Image to ImageJ: 25 years of image analysis. Nat Methods. 2012.

[6] Schindelin J, Arganda-Carreras I, Frise E, Kaynig V, Longair M, Pietzsch T, *et al*. Fiji: an open-source platform for biological-image analysis. Nat Methods. 2012;9:676–682.